Biosensors and Bioelectronics 142 (2019) 111557

Contents lists available at ScienceDirect

Biosensors and Bioelectronics

journal homepage: www.elsevier.com/locate/bios

Beta-cyclodextrin-functionalized CdS nanorods as building modules for ultrasensitive photoelectrochemical bioassay of HIV DNA

Jing Fan[a], Yang Zang[a,*], Jingjing Jiang[a], Jianping Lei[b,**], Huaiguo Xue[a]

[a] School of Chemistry and Chemical Engineering, Yangzhou University, Yangzhou, Jiangsu, 225002, PR China
[b] State Key Laboratory of Analytical Chemistry for Life Science, School of Chemistry and Chemical Engineering, Nanjing University, Nanjing, Jiangsu, 210023, PR China

ARTICLE INFO

Keywords:
Photoelectrochemistry
Biosensor
CdS
Beta-cyclodextrin
DNA

ABSTRACT

Nowadays, acquired immunodeficiency syndrome has become a formidable danger to human health, and its early diagnosis is urgent need with the increasing quantity of patients around the world. Herein, we first synthesized beta-cyclodextrin-functionalized CdS nanorods (β-CD@CdS NRs) with high stability and desirable photo-electricity activity, and served as easy-to-assemble building modules to design a novel photoelectrochemical biosensor for human immune deficiency virus (HIV) DNA detection by coupling with catalytic hairpin assembly (CHA)-mediated biocatalytic precipitation and the host-guest interaction between adamantine (ADA) and β-CD. In the presence of HIV DNA, CHA process was triggered with the aid of hairpin DNA1 and ADA-labelled hairpin DNA2, and then generated large amounts of G-quadruplex, which could be formed hemin/G-quadruplex DNAzyme to catalyze 4-chloro-1-naphthol to generate insoluble precipitation on photoelectrode surface, followed by the decreased photocurrent response due to the corresponding stereo-hindrance effect. Under optimized conditions, this biosensor exhibited wide linear dynamic range (10 fM – 1 nM) and low detection limit of 1.16 fM, as well as high sensitivity, excellent stability, and satisfactory feasibility in human-serum samples. Moreover, the prepared β-CD@CdS NRs could be applied to the construction of other advanced sensing platform, showing great prospect in clinical diagnostics.

1. Introduction

Acquired immunodeficiency syndrome (AIDS) caused by human immune deficiency virus (HIV), has been identified as one of the most serious diseases that threaten human health due to its severe infectivity and high fatality rate (Fang et al., 2018; Huang et al., 2017). The early diagnosis of AIDS is urgent for medical organization to save unknown infected persons and protect healthy peoples (Shamsipur et al., 2019). So far, several detection techniques, such as electrochemistry, dynamic light scattering, fluorescence and photoelectrochemistry (PEC)-based biosensing (Akiyama et al., 2018; Gao et al., 2018; Wang et al., 2015; Ye et al., 2016; Zou and Ling, 2018), have been developed for the direct detection of HIV DNA without the impact of "window period" (Li et al., 2014), which efficiently avoids the disadvantage of traditional blood tests (e.g. high cost, long analysis time and dedicated equipment). Among them, photoelectrochemical bioanalysis has become a burgeoning sensing method for DNA monitoring owing to its high sensitivity and low background (Shi et al., 2016; Wen et al., 2018; Zang et al., 2016), in which its biochemical information can be monitored by photocurrent change stemmed from target-triggered recognition event under light irradiation (Li et al., 2016; Saha et al., 2018), avoiding the high cost and time consuming of other detection techniques including mass spectrometry and Raman spectroscopic analysis (Otange et al., 2017; Rejeeth et al., 2018). And an outstanding photoactive material has become a key indicator for advanced photoelectrochemical devices. However, most of photoactive materials suffer from low light conversion efficiency, easy to photocorrosion and unsatisfactory biocompatibility (Li et al., 2017; Zang et al., 2018).

At present, several photoactive materials with unique morphology have gained extensive attention by means of their wonderful durability and photocatalytic activity (Li et al., 2019; Liang et al., 2019; Wang et al., 2018a, 2018c). Among them, CdS nanorods (NRs), as outstanding narrow-gap semiconductors, exhibit a huge potential in photocatalysis and photoelectrochemical bioassays through reducing the carrier radial transmission distance and enhancing the active site of PEC reaction (Wang et al., 2018b; Wolff et al., 2018). For example, Tang et al. proposed a photoelectrochemical assay of prostate-specific antigen based on CdS NRs and rolling circle amplification (Zhang et al., 2018a).

* Corresponding author.
** Corresponding author.
E-mail addresses: zangyang@yzu.edu.cn (Y. Zang), jpl@nju.edu.cn (J. Lei).

https://doi.org/10.1016/j.bios.2019.111557
Received 24 April 2019; Received in revised form 13 July 2019; Accepted 30 July 2019
Available online 01 August 2019
0956-5663/

However, the further application of bare CdS NRs in biological analysis is restricted by difficult-to-bind biorecognition probe. Fortunately, β-cyclodextrin (β-CD) as a satisfactory host molecule can be modified onto nanoparticles surface to bind various guest molecule-labeled biological probes via strong host-guest recognition ability (Gao et al., 2015; Xie et al., 2018). And the introduction of β-CD will not only improve the solubility and stability of CdS NRs (Hu et al., 2014), but also provide enough recognition sites for DNA assembly on electrode interface, which is suitable for the construction of high-powered photoelectrochemical sensing devices with desirable photoactive materials and simplified interface modification procedures (Yang et al., 2015).

In addition to high-performance semiconductor nanomaterials, DNA assembly technologies also provide a new conversion mode for enhancing photocurrent signal (Chu et al., 2019; Li et al., 2018a; Zhang et al., 2018b). Especially, catalyzed hairpin assembly (CHA) as an enzyme-free amplification strategy is widely favored by analysts because of its low background interference, high programmability and hundred-fold amplification factor, which can be elevated the detection performance of biosensor by CHA-mediated DNA structure transformation and signaling cascade (Chen et al., 2018b; Li et al., 2018b; Xiong et al., 2018). For instance, Yuan et al. reported a sensitive DNA biosensor by dual-amplification strategy of 3D DNA walking machine and CHA recycling (Qing et al., 2018). Considering the advantages of β-CD@CdS NRs and CHA, a novel photoelectrochemical biosensor can be designed for trace DNA detection.

In this work, we first synthesize β-CD@CdS NRs by solvothermal method, and develop an ultrasensitive photoelectrochemical biosensor for HIV DNA (T_{HIV}) monitoring based on the signal amplification of CHA-mediated the formation of hemin/G-quadruplex DNAzyme and biocatalytic precipitation (BCP) (Scheme 1). The prepared β-CD@CdS NRs as efficient building modules not only act as signal element for photocurrent generation but also immobilize adamantine-labeled hairpin DNA2 (ADA-H_2) probe via host-guest interaction. In the presence of HIV DNA, hairpin DNA1 (H_1) can be opened by DNA hybridization, and then initiates the CHA cyclic process with the aid of ADA-H_2 so that a large amount of G-quadruplex was generated with the structure transformation of H_1:ADA-H_2 conjugates. After bound with hemin molecules, the formed hemin/G-quadruplex DNAzyme can catalyze 4-chloro-1-naphthol (4-CN) to form insoluble precipitation on electrode surface, resulting in the decrease of photocurrent, along with the effective inhibition of the diffusion and electron transition of ascorbic acid (AA) by steric hindrance. Thus, based on the desirable photoelectric property and easy to assemble of β-CD@CdS NRs and the signaling cascade of CHA-stimulated DNAzyme catalysis, this biosensor can detect trace HIV DNA, and successfully applied in real human serum analysis, showing great promising in early diagnostics of AIDS.

2. Experimental section

2.1. Materials and reagents

Indium tin oxide (ITO) electrodes were bought from Zhuhai Kaivo Electronic Components Co. Ltd. (China). Ethylenediamine, cadmium nitrate tetrahydrate [$Cd(NO_3)_2{\cdot}4H_2O$] and thiourea [$SC(NH_2)_2$] were purchased from Sinopharm Chemical Reagent Co., Ltd. (China). 1-ethyl-3-(3-(dimethylamino)propyl) carbodiimide (EDC) and N-hydroxysuccinimide (NHS) were obtained from Sigma-Aldrich Chemical Co. (USA). Carboxymethyl-β-cyclodextrin (CM-β-CD) was bought from Zhiyuan Biotechnology Co., Ltd. (China). 1 × TE buffer (pH 8.0), bovine serum albumin (BSA) and AA were purchased from Sangon Biotech. Co., Ltd (Shanghai, China). All the reagents were of analytical grade and used without further purification. All aqueous solutions were prepared using deionized water from a Millipore water purification system (≥ 18 MΩ cm, Milli-Q, Millipore). Nucleic acids used in this work were purchased from Takara Biotech. Co., Ltd. (Dalian, China), and the corresponding sequences were displayed in Table S1. All DNA sequences were dissolved into 1 × TE buffer before usage, and DNA assembly processes and electrode washing were performed in 10 mM Tris-HCl buffer of pH 7.4 containing 5 mM $MgCl_2$ and 20 mM KCl. Prior to experiments, H_1 and ADA-H_2 were annealed at 90 °C for 5 min followed by cooling naturally to room temperature.

2.2. Apparatus

Transmission electron micrographs (TEM) were performed by a JEM-2100 transmission electron microscope (Jeol, Japan). Energy

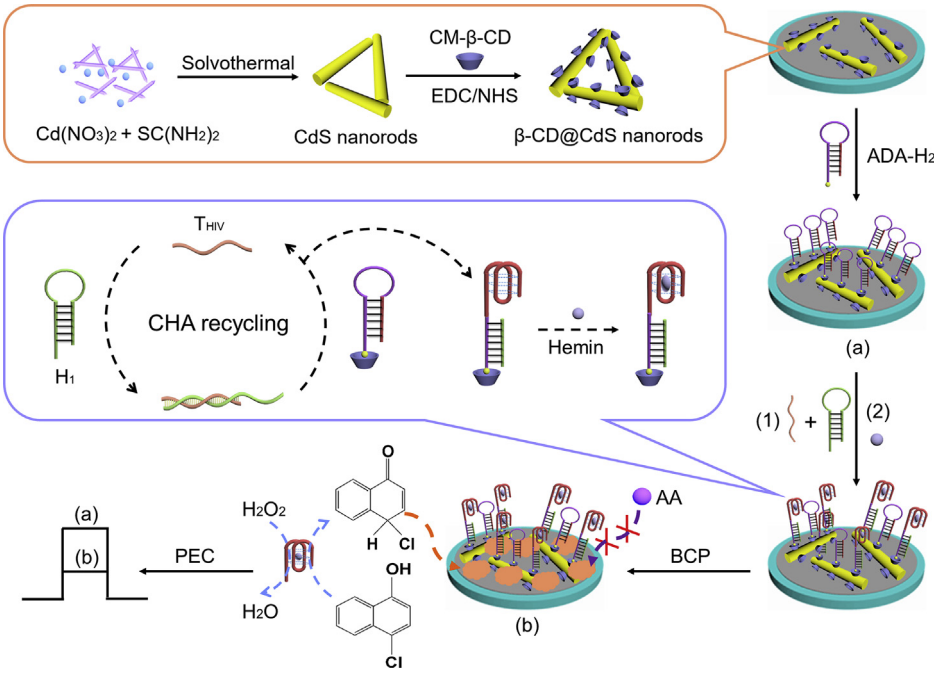

Scheme 1. Schematic illustration of the preparation of β-CD@CdS NRs, and stepwise assembly process for photoelectrochemical bioassay of T_{HIV} based on CHA-mediated enzymatic reaction.

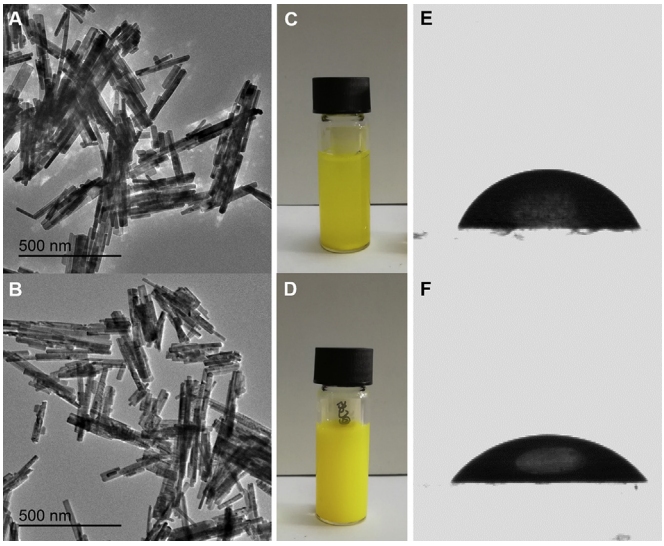

Fig. 1. TEM images of (A) CdS NRs and (B) β-CD@CdS NRs. The water solubility images and static water contact angles for 1 mg mL^{-1} (C, E) CdS NRs and (D, F) β-CD@CdS NRs, respectively.

dispersive X-ray spectroscopy (EDS) was observed by a Zeiss Supra55 field emission scanning electron microscope (Zeiss, Germany). Contact angles were measured by an OCA20 video optical contact angle measuring instrument (Dataphysics, Germany). X-ray photoelectron spectroscopy (XPS) experiments were carried out on an ESCALAB 250Xi spectrometer (Thermo Fisher, USA) with an Al *Kα* radiation source. The Fourier transform infra-red (FTIR) spectra were characterized by Tensor 27 Fourier transform infrared spectrometer (Bruker, Germany). X-ray power diffraction (XRD) patterns were obtained by D8 Advance X-Ray diffractometer (Bruker, Germany). Circular dichroism (CD) spectra were performed on a J-810 circular dichroism spectrometer (Jasco, Japan). UV–vis absorption spectra were obtained by an UV-2501PC fluorescence spectrometer (Shimadzu, Japan). Photoelectrochemical experiments were recorded by a CHI 660E electrochemical workstation (Chenhua, China) as home-built PEC system with white light as an accessory excitation source. Electrochemical impedance spectroscopy (EIS) was tested by a PGSTAT30/FRA2 system (Autolab, The Netherlands) in 0.1 M Na_2SO_4 solution containing 5 mM $[Fe(CN)_6]^{3-/4-}$, and the applied potential is 0.180 V with the signal amplitude of 5 mV and the frequency range from 0.1 Hz to 100 kHz. All electrochemical and photoelectrochemical experiments were carried out at room temperature using a conventional three-electrode system: a modified ITO electrode (4 mm in diameter) as the working, a platinum electrode as the auxiliary, and an Ag/AgCl as the reference electrodes.

2.3. Synthesis of CdS NRs and β-CD@CdS NRs

CdS NRs were prepared by a facile hydrothermal reaction (Yin et al., 2016). Typically, 2.5 g $Cd(NO_3)_2{\cdot}4H_2O$ and 1.85 g $SC(NH_2)_2$ were dissolved into 40 mL ethylenediamine, and vigorously stirred for 30 min at room temperature to yield a homogeneous mixture, which was then transferred to a 100 mL Teflon-lined autoclave and kept at 160 °C for 24 h to generate a bright yellow suspension. After natural cooling, the above suspension was rinsed with deionized water and absolute ethanol for several times in a centrifugal machine, and then pure CdS NRs was obtained by centrifugation and drying in vacuum drying oven at 60 °C.

Moreover, as-prepared CdS NRs and excess CM-β-CD were dispersed into 10 mM PBS buffer of pH 5.3 containing 20 mM NHS and 10 mM EDC and stirred for 12 h at room temperature, β-CD@CdS NRs were synthesized after being rinsed and dried at 60 °C.

2.4. Construction of photoelectrochemical biosensor

ITO electrodes were cut into 10 × 45 mm slices, and cleaned by ultrasonic treatment in 1 M NaOH, H_2O_2 (10%), ethanol and deionized water twice for 30 min, respectively. After being washed by deionized water and blow-dried with nitrogen, 10 μL β-CD@CdS NRs (0.5 mg mL^{-1}) was drew to ITO electrode surface and dried at room temperature. Then, 10 μL ADA-H_2 was dropped onto modified electrode surface to incubate for 1 h, and washed three times by electrode lotion to remove the non-conjugated DNA. Finally, the unbound sites of β-CD@CdS NRs were blocked by 1% (w/v) BSA solution during the incubation time of 40 min, and the prepared electrode was marked as BSA/ADA-H_2/β-CD@CdS NRs.

2.5. Photoelectrochemical measurements

10 μL of 10 mM Tris buffer (pH 7.4) containing H_1 and different concentrations of T_{HIV} was applied onto BSA/ADA-H_2/β-CD@CdS electrode surface and incubated for 2 h. Then, hemin/G-quadruplex DNAzyme was formed by the addition of 4 μM hemin solution onto the above electrode for 40 min. After incubation with 0.1 M PBS of pH 7.4 containing 1.0 mM 4-CN and 0.01 mM H_2O_2 for 10 min, the modified electrode was covered by insoluble sediment. Finally, PEC measurements were performed in 0.1 M PBS of pH 7.4 containing 0.1 M AA for at bias voltage of 0 V (versus Ag/AgCl). And, more remarkable, the modified electrode was rinsed with washing buffer after each modification step.

3. Results and discussion

3.1. Characterizations of CdS NRs and β-CD@CdS NRs

Fig. 1A and Fig. 1B presented the TEM images of CdS NRs and β-CD@CdS NRs, respectively. As can be seen, CdS NRs showed the typical rod-like structure with a diameter range from 25 nm to 40 nm. After subsequent modification of β-CD, the morphology and size of β-CD@CdS NRs were not obviously affected, but exhibited the better disperse ability, revealing more active sites for DNA assembly as building modules. Meanwhile, the aqueous solution of β-CD@CdS NRs was more homogeneous and stable than that of CdS NRs under the same concentration (Fig. 1C and D) due to the introduction of β-CD, which was further confirmed by contact angle testing. As displayed in Fig. 1E and Fig. 1F, the contact angles of CdS NRs and β-CD@CdS NRs were 64.4° and 52.6°, respectively, and these results indicated that the hydrophilicity of CdS NRs could be improved apparently after the modification of β-CD.

EDS measurements were performed to explore the chemical composition of both CdS NRs. As depicted in Fig. 2A, the characteristic peaks of S and Cd elements could be observed from CdS NRs, and the existence of C and O elements was ascribed to the remnant $Cd(NO_3)_2$ and $SC(NH_2)_2$ (curve a). Yet for β-CD@CdS NRs, the peak intensity of C element was greatly increased compared to that of CdS NRs (curve b), as well as the marginal improvement for O element, which was attributed to the successful inclusion of β-CD on CdS NRs surface. Similarly, from XPS analyses we also found the corresponding characteristic peaks of the above elements (Fig. 2B). Compared with the C and O signals of CdS NRs at 284.9 eV and 531.0 eV (curve a), that of β-CD@CdS NRs at 286.1 eV and 532.1 eV were sharp elevated (curve b). And their positive shifts revealed the possible interaction between β-CD and CdS NRs.

Fig. 2C presented the spectra of CdS NRs, CM-β-CD and β-CD@CdS NRs. In the spectrum for CdS NRs (curve a), the characteristic stretching bands of N–H were found at 3334 and 3248 cm^{-1}, respectively, as well as the corresponding N–H bending vibration at 1587 cm^{-1}, demonstrating the existence of $–NH_2$ on CdS NRs surface. In the spectrum for CM-β-CD (curve b), a typical band at 3100–3670 cm^{-1} was observed

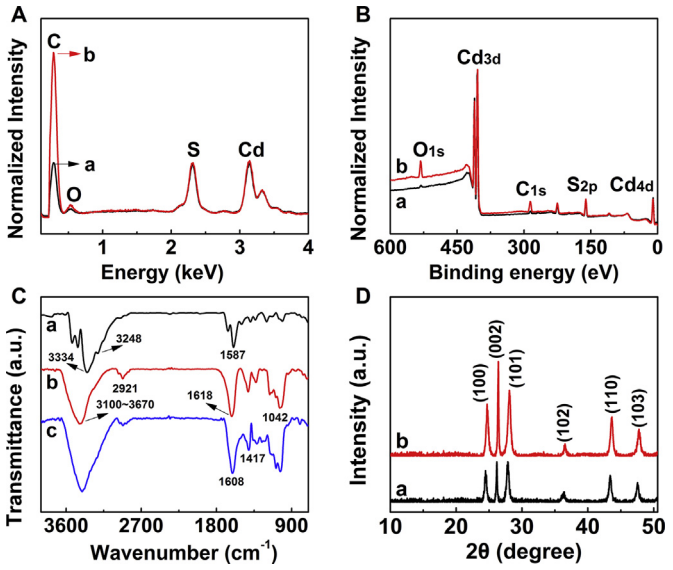

Fig. 2. (A) EDS and (B) XPS survey spectra of CdS NRs (a) and β-CD@CdS NRs (b). (C) FTIR spectra of CdS NRs (a), CM-β-CD (b) and β-CD@CdS NRs (c). (D) XRD patterns of CdS NRs (a) and β-CD@CdS NRs (b).

due to the presence of –OH stretching vibration, accompanied by C–H stretching band at 2921 cm^{-1}, C = O stretching band at 1618 cm^{-1}, and C–O–C stretching band at 1042 cm^{-1} (Ghosh et al., 2011). After the introduction of CM-β-CD, the C = O stretching band of β-CD@CdS NRs was shifted to 1608 cm^{-1} (curve c), and C–N stretching band existed at 1417 cm^{-1}, which also proved that CM-β-CD had been grafted onto CdS NRs surface by amidation reaction (Jiang et al., 2018).

The crystalline structures of as-synthesized CdS NRs and β-CD@CdS NRs were studied by XRD patterns (Fig. 2D). As displayed in curve a, the typical XRD peaks of CdS NRs located at 24.8°, 26.5°, 28.2°, 36.6°, 43.7°, 47.8° could be well-indexed as (100), (002), (101), (102), (110), (103) planes of hexagonal phase (Chen et al., 2018a). Likewise, there was no shift of peak positions for hexagonal β-CD@CdS NRs (curve b), revealing that β-CD molecules could get assembled on CdS NRs surface, and no obvious structure variation occurred after the modification of β-CD.

3.2. Feasibility of photoelectrochemical biosensor

To prove the successful fabrication of designed biosensor, we have recorded the photocurrent responses of modified electrodes under each modification step (Fig. 3A). It can be seen from the figure that the photocurrent reached the maximum value when the electrode surface was modified with β-CD@CdS NRs (curve a). As ADA-H_2 and BSA were stepwise modified, followed by CHA-modulated G-quadruplex and hemin/G-quadruplex formation, the photocurrent declined in turn owing to the increase of steric hindrance (curves b–e). Subsequently, the insulating precipitation generated by enzymatic reaction thwarted the migration and electron transfer of electron donor from electrolyte to photoanode surface, resulting in a further reduction of photocurrent response (curve f). Furthermore, EIS measurements were also carried out to test the assembly process of biosensor. As displayed in Fig. 3B, charge transfer resistance (R_{ct}) of bare ITO electrode was 116.9 Ω (curve a), and the R_{ct} value of modified electrode increased gradually from 338.4 Ω to 775.5 Ω (curves b–f) with the layer-by-layer assembly of β-CD@CdS NRs, ADA-H_2, BSA, H_1 and hemin molecules. After the precipitation was formed by DNAzyme catalysis in 4-CN/H_2O_2 system, R_{ct} value reached 1009.1 Ω (curve g). These results indicated that the fabrication and detection of biosensor were feasible.

From CD spectra (Fig. 3C), it can be seen that H_1, ADA-H_2, H_1 + T_{HIV} have obvious negative peaks at 241 nm compared to single

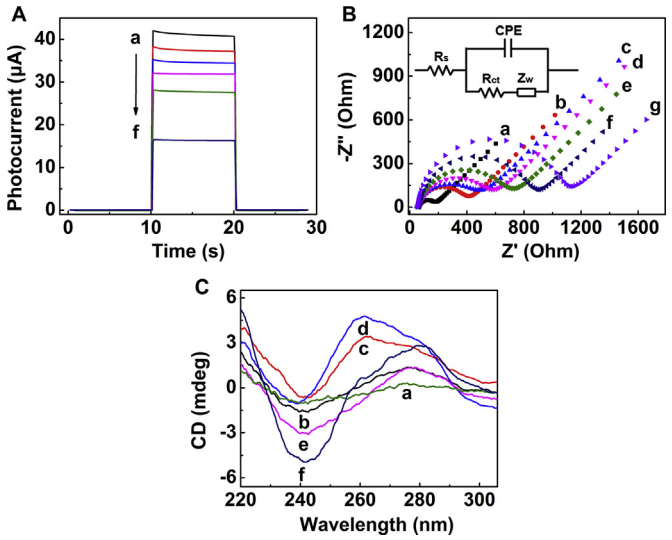

Fig. 3. (A) Photocurrent responses of ITO electrodes after the stepwise assembly of β-CD@CdS NRs (a), ADA-H_2 (b), BSA (c), CHA-triggered G-quadruplex-ADA-H_2:H_1 (d), hemin (e), and hemin/G-quadruplex-based BCP (f). (B) EIS of bare ITO electrode (a), and (a) after the stepwise modification of β-CD@CdS NRs (b), ADA-H_2 (c), BSA (d), CHA-triggered G-quadruplex-ADA-H_2:H_1 (e), hemin (f), and hemin/G-quadruplex-based BCP (g). Inset: The electrical equivalent circuit applied to fit the impedance data; R_s, Z_w, R_{ct}, and CPE represent the Ohmic resistance of the electrolyte, Warburg impedance, charge-transfer resistance, and constant phase angle element, respectively. (C) CD spectra of (a) 2 μM T_{HIV}, (b) 2 μM H_1, (c) 2 μM ADA-H_2, (d) 2 μM H_1 + 2 μM ADA-H_2, (e) 2 μM H_1 + 2 μM T_{HIV}, and (f) 2 μM H_1 + 2 μM ADA-H_2 + 2 μM T_{HIV}.

T_{HIV} due to the existence of long double-strand DNA fragment (curves a–c, e), as well as the increased peak strength for the mixture of H_1 and ADA-H_2 (curve d). Moreover, when T_{HIV} and H_1 were added into ADA-H_2 solution (curve f), the positive peak at 281 nm was appeared with the elevation of the negative peak at 241 nm, which was consistent with the characteristics peak of DNA G-quadruplex and double-strand DNA structure, respectively, indicating that CHA recycling triggered by T_{HIV} has progressed as expected (Han et al., 2019; Nakayama and Sintim, 2009).

3.3. Optimization of experimental conditions

The key experimental parameters that influenced the analytical results of biosensor, such as ADA-H_2 concentration, binding time between hemin and G-quadruplex for DNAzyme generation, and reaction time of BCP, were systematically optimized for T_{HIV} assay (Fig. S1). It can be seen from Fig. S1A that the photocurrent signal declined with the increasing ADA-H_2 content from 0.25 μM to 1.0 μM, and then elevated slightly when its concentration continued to ascend, which suggested that excess ADA-H_2 probe on electrode surface might suppress the subsequent CHA reaction. Therefore, 1.0 μM was chosen for the optimal concentration of ADA-H_2. The influence of hemin incubation time on the amount of formed hemin/G-quadruplex DNAzyme was further measured. As illustrated in Fig. S1B, the photocurrent response decreased gradually from 10 min to 40 min, and then tended to a plateau owing to the attainment of reaction equilibrium, so 40 min was selected as the optimal time. Furthermore, the sensing property of biosensor was affected by the catalytic time of BCP reaction (Fig. S1C). The photocurrent decreased with the prolongation of catalytic time up to 10 min, and showed a stable trend for the extension of time. Thus, 10 min was suitable for the catalytic oxidation of 4-CN.

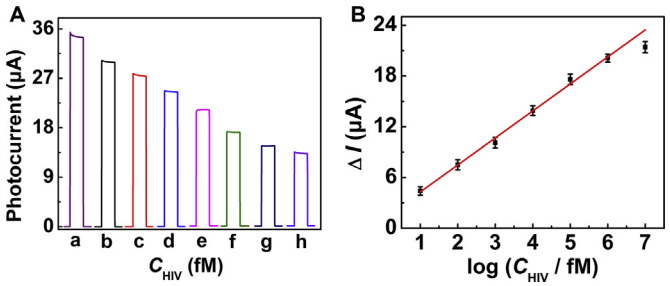

Fig. 4. (A) Photocurrent responses of the proposed biosensor at different concentrations of T_{HIV}: 0 (a), 0.01 (b), 0.1 (c), 1 (d), 10 (e), 100 (f), 1000 (g), and 10000 (h) pM, respectively. (B) The corresponding calibration curve.

3.4. Analytical performance of developed biosensor

To investigate the detection properties of biosensor via CHA-triggered BCP on β-CD@CdS NRs surface, the photocurrent measurements toward different T_{HIV} concentrations were carried out under the optimized conditions (Fig. 4A). The photocurrent declined dramatically with incremental target concentration because of the enhanced coverage of insoluble sediment, and the linear dynamic range of biosensor was obtained from 10 fM to 1 nM (Fig. 4B), which was wider than the impedimetric sensing via graphene-nafion composite (100 fM – 100 pM) (Gong et al., 2017), and fluorescent biosensor based on DNA walker-modulated cascade amplification (5 fM – 1.67 pM) (Zheng et al., 2018). The fitting equation expressed as ΔI (μA) = 1.08 + 3.19 lgC_{HIV} (fM) with a correlation coefficient of 0.9967 ($\Delta I = I_0 - I$; I_0 represented the photocurrent response of biosensor before the addition of target, and I represented that of biosensor after BCP reaction). The detection limit was estimated to be 1.16 fM at 3σ, and this value was lower than 15 fM for fluorescent bioassay by means of resonance energy transfer between gold nanoparticles and carbon dots (Qaddare and Salimi, 2017), and 48 fM for surface plasmon resonance sensor through entropy-driven strand displacement reactions (Diao et al., 2018). The analytical performance of developed biosensor was also compared with that of more reported works using different methods (Table S2). Obviously, the satisfactory detection results and high sensitivity of our work were attributed to the excellent host-guest recognition and photoelectric properties of β-CD@CdS NRs, as well as CHA-initiated the formation of hemin/G-quadruplex DNAzyme.

Selectivity of the biosensor was tested by photocurrent changes toward different DNA sequences including T_{HIV}, single-base (T_1) and three-base (T_3) mismatched DNA. It can be seen from Fig. 5A that the ΔI of T_{HIV} was 18.2 μA, which was 6.5 and 15.2 times higher than that of T_1 and T_3, respectively, because base-mismatched DNAs could not be efficiently hybridized with H_1 to initiate the following CHA and BCP processes. Obviously, these results proved the outstanding specificity for HIV DNA against base-mismatched DNAs by means of the reliable programmability and recognition capability of CHA-modulated cascade signal amplification.

To test the reproducibility of proposed strategy, time-based photocurrent response of biosensor under continuous "off-on-off" light irradiation for 10 cycles was displayed in Fig. 5B. We found that the photocurrent did not significant change as the light switched repeatedly, indicating a desirable stability and reproducibility for HIV DNA assay. In addition, the relative standard deviation (RSD) of five duplicate photoelectrochemical measurements was 4.7% for 100 pM, and the detected photocurrent remained 96.9% and 95.2% of its initial value when the well-prepared biosensor was kept under 4 °C for 9 and 15 days (Fig. 5C). These results demonstrated that β-CD@CdS NRs-based biosensor possessed an acceptable reproducibility and storage stability.

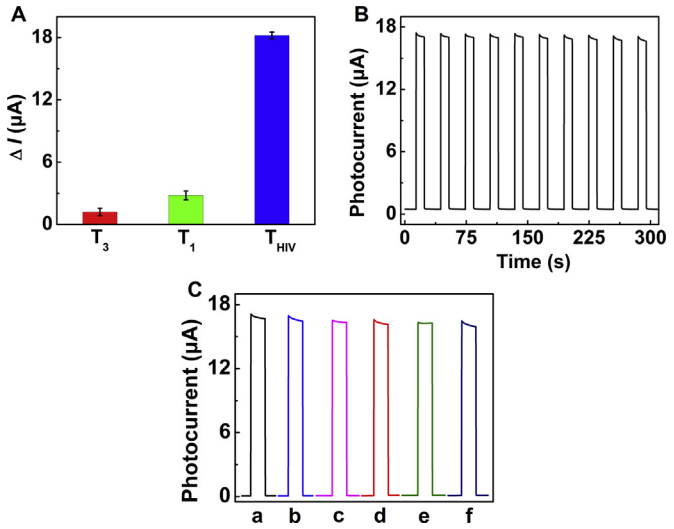

Fig. 5. (A) Specificity of the proposed biosensor for T_{HIV} in comparison to single-base and three-base mismatched DNAs at 100 pM level. (B) Time-based photocurrent response of the designed biosensor. (C) Photocurrent responses of the designed biosensor after kept at 4 °C for 0 (a), 3 (b), 6 (c), 9 (d), 12 (e), and 15 (f) days.

3.5. Analysis of T_{HIV} in human serum samples

By means of standard addition method, the applicability of designed biosensor for T_{HIV} assay was further explored in real human serum samples from Medical and Health Center of Yangzhou University, which were diluted 100 times to avoid the influence of high concentration tissue on DNA hybridization efficiency. As shown in Table S3, when spiked with 0.1, 1, 10, 100 and 1000 pM T_{HIV} standard solutions, the average recoveries from 96.2% to 105.7% (n = 5) were recorded and the corresponding RSD was no more than 6.49%, showing acceptable precision and great potential in clinical application.

4. Conclusion

In summary, we successfully synthesized β-CD@CdS NRs as stable and easy-to-assemble building modules for the ultrasensitive photoelectrochemical detection of HIV DNA. The β-CD@CdS NRs with desirable dispersibility and water solubility could remarkably improve the film-forming property of CdS NRs, accelerate the electron transfer and separation efficiency of photogenerated charge carriers, and was favorable for binding DNA probe via host-guest interaction. With the successful modification of ADA-H_2 onto electrode surface, CHA recycling was triggered to generate G-quadruplex in the presence of H_1 and T_{HIV}, and hemin/G-quadruplex DNAzyme was then formed after the introduction of hemin. And, the photocurrent signal greatly weakened when non-conductive substances that generated by enzyme catalysis reaction efficiently hindered the interfacial diffusion and electron transfer of AA. The designed biosensor exhibited high selectivity, excellent stability and satisfactory reproducibility, which could be quantitative detection of T_{HIV} at five orders of magnitude with detection limit down to fM level, and achieved extensive prospect in real human serum sample detection. Moreover, such β-CD@CdS NRs as building modules could construct various advanced sensing platform in the application of environment and biomedical analysis.

CRediT authorship contribution statement

Jing Fan: Formal analysis, Data curation, Writing - original draft. **Yang Zang:** Conceptualization, Formal analysis, Writing - original draft, Writing - review & editing, Funding acquisition. **Jingjing Jiang:** Formal analysis, Funding acquisition. **Jianping Lei:** Conceptualization,

Formal analysis, Writing - review & editing. **Huaiguo Xue:** Formal analysis, Resources, Project administration.

Acknowledgements

This work was supported by the National Natural Science Foundation of China (Grants: 21605129, 21703199), and China Postdoctoral Science Foundation (Grant: 2017M621830). The authors also acknowledge the Testing Center of Yangzhou University for TEM and XPS measurements.

Appendix A. Supplementary data

Supplementary data to this article can be found online at https://doi.org/10.1016/j.bios.2019.111557.

Declaration of interests

The authors declare that they have no known competing financial interests or personal relationships that could have appeared to influence the work reported in this paper.

References

Akiyama, H., Miller, C.M., Ettinger, C.R., Belkina, A.C., Snyder-Cappione, J.E., Gummuluru, S., 2018. Nat. Commun. 9, 3450.
Chen, W., Wang, Y.H., Liu, M., Gao, L., Mao, L.Q., Fan, Z.Y., Shangguan, W.F., 2018a. Appl. Surf. Sci. 444, 485–490.
Chen, Y.X., Wu, X., Huang, K.J., 2018b. Sens. Actuators B Chem. 270, 179–186.
Chu, Y.X., Deng, A.P., Wang, W.J., Zhu, J.J., 2019. Anal. Chem. 91, 3169–3627.
Diao, W., Tang, M., Ding, S.J., Li, X.M., Cheng, W.B., Mo, F., Yan, X.Y., Ma, H.M., Yan, Y.R., 2018. Biosens. Bioelectron. 100, 228–234.
Fang, B.Y., Li, C., An, J., Zhao, S.D., Zhuang, Z.Y., Zhao, Y.D., Zhang, Y.X., 2018. Nanoscale 10, 5532–5538.
Gao, J., Guo, Z.K., Su, F.J., Gao, L., Pang, X.H., Cao, W., Du, B., Wei, Q., 2015. Biosens. Bioelectron. 63, 465–471.
Gao, X.Y., Wang, X.L., Li, Y.C., He, J.L., Yu, H.Z., 2018. Anal. Chem. 90, 8147–8153.
Ghosh, S., Badruddoza, A.Z.M., Uddin, M.S., Hidajat, K.J., 2011. Colloid Interface Sci. 354, 483–492.
Gong, Q.J., Wang, Y.D., Yang, H.Y., 2017. Biosens. Bioelectron. 89, 565–569.
Han, Y.P., Zhang, F., Gong, H., Cai, C.Q., 2019. Sens. Actuators B Chem. 281, 303–310.
Hu, Q.D., Tang, G.P., Chu, P.K., 2014. Acc. Chem. Res. 47, 2017–2025.
Huang, Y.L., Gao, Z.F., Luo, H.Q., Li, N.B., 2017. Sens. Actuators B Chem. 238, 1017–1023.
Jiang, J.J., Lin, X.Y., Ding, D., Diao, G.W., 2018. Biosens. Bioelectron. 114, 37–43.
Li, B., Li, Z.L., Situ, B., Dai, Z., Liu, Q.L., Wang, Q., Gu, D.Y., Zheng, L., 2014. Biosens. Bioelectron. 52, 330–336.
Li, L., Zheng, X.X., Huang, Y.Z., Zhang, L.N., Cui, K., Zhang, Y., Yu, J.H., 2018a. Anal. Chem. 90, 13882–13890.
Li, M.J., Liang, W.B., Yuan, R., Chai, Y.Q., 2019. ACS Appl. Mater. Interfaces 11, 11834–11840.
Li, N.X., Du, M.Y., Liu, Y.C., Ji, X.H., He, Z.K., 2018b. ACS Sens. 3, 1283–1290.
Li, R.Y., Yan, R., Bao, J.C., Tu, W.W., Dai, Z.H., 2016. Chem. Commun. 52, 11799–11802.
Li, X., Zhu, L.S., Zhou, Y.L., Yin, H.S., Ai, S.Y., 2017. Anal. Chem. 89, 2369–2376.
Liang, Q., Cui, S.N., Liu, C.H., Xu, S., Yao, C., Li, Z.Y., 2019. Chem. Eng. J. 364, 102–110.
Nakayama, S., Sintim, H.O., 2009. J. Am. Chem. Soc. 131, 10320–10333.
Otange, B.O., Birech, Z., Okonda, J., Rop, R., 2017. Anal. Bioanal. Chem. 409, 3253–3259.
Qaddare, S.H., Salimi, A., 2017. Biosens. Bioelectron. 89, 773–780.
Qing, M., Xie, S.B., Cai, W., Tang, D.Y., Tang, Y., Zhang, J., Yuan, R., 2018. Anal. Chem. 90, 11439–11445.
Rejeeth, C., Pang, X.C., Zhang, R., Xu, W., Sun, X.M., Liu, B., Lou, J.T., Wan, J.J., Gu, H.C., Yan, W., Qian, K., 2018. Nano Res. 11, 68–79.
Saha, S., Chan, Y.T., Soleymani, L., 2018. ACS Appl. Mater. Interfaces 10, 31178–31185.
Shamsipur, M., Samandari, L., Taherpour, A., Pashabadi, A., 2019. Anal. Chim. Acta 1055, 7–16.
Shi, X.M., Fan, G.C., Shen, Q.M., Zhu, J.J., 2016. ACS Appl. Mater. Interfaces 8, 35091–35098.
Wang, J., Liu, Z.H., Hu, C.G., Hu, S.S., 2015. Anal. Chem. 87, 9368–9375.
Wang, J., Xu, Q., Xia, W.W., Shu, Y., Jin, D.Q., Zang, Y., Hu, X.Y., 2018a. Sens. Actuators B Chem. 271, 215–224.
Wang, L.J., Wang, W.Z., Chen, Y.L., Yao, L.Z., Zhao, X., Shi, H.L., Cao, M.S., Liang, Y.J., 2018b. ACS Appl. Mater. Interfaces 10, 11652–11662.
Wang, R.Y., Li, X.D., Wang, L., Zhao, X.R., Yang, G.C., Li, A.D., Wu, C.P., Shen, Q., Zhou, Y., Zou, Z.G., 2018c. Nanoscale 10, 19621–19627.
Wen, G.M., Dong, W.X., Liu, B., Li, Z.P., Fan, L.F., 2018. Biosens. Bioelectron. 117, 91–96.
Wolff, C.M., Frischmann, P.D., Schulze, M., Bohn, B.J., Wein, R., Livadas, P., Carlson, M.T., Jäckel, F., Feldmann, J., Würthner, F., Stolarczyk, J.K., 2018. Nat. Energy 3, 862–869.
Xie, X.Y., Wang, H.J., Zhang, L., Liu, Y.T., Chai, Y.Q., Yuan, Y.L., Yuan, R., 2018. Sens. Actuators B Chem. 258, 1146–1151.
Xiong, E.H., Zhen, D.S., Jiang, L., 2018. Chem. Commun. 54, 12594–12597.
Yang, M., Wang, Y., Wang, H.Y., 2015. Electrochim. Acta 169, 7–12.
Ye, Y.D., Xia, L., Xu, D.D., Xing, X.J., Pang, D.W., Tang, H.W., 2016. Biosens. Bioelectron. 85, 837–843.
Yin, X.L., Li, L.L., Jiang, W.J., Zhang, Y., Zhang, X., Wan, L.J., Hu, J.S., 2016. ACS Appl. Mater. Interfaces 8, 15258–15266.
Zang, Y., Fan, J., Ju, Y., Xue, H.G., Pang, H., 2018. Chem. Eur J. 24, 1–19.
Zang, Y., Lei, J.P., Hao, Q., Ju, H.X., 2016. Biosens. Bioelectron. 77, 557–564.
Zhang, K.Y., Lv, S.Z., Lin, Z.Z., Li, M.J., Tang, D.P., 2018a. Biosens. Bioelectron. 101, 159–166.
Zhang, K.Y., Lv, S.Z., Lu, M.H., Tang, D.P., 2018b. Biosens. Bioelectron. 117, 590–596.
Zheng, J., Ji, X.H., Du, M.Y., Tian, S.B., He, Z.K., 2018. Nanoscale 10, 17206–17211.
Zou, L., Ling, L.S., 2018. Anal. Chem. 90, 13373–13377.